Utilizing Microfabrication Techniques to Develop a Flow Cytometer on a Chip

Zan Chaudhry
Department of Biomedical Engineering, Johns Hopkins University, Baltimore, USA

***Abstract*—Flow cytometry is an increasingly important technique for biological research applications. Additionally, flow cytometry provides more sophisticated cell-based diagnostic tools for clinical settings. However, current technology is large and expensive, costing tens to hundreds of thousands of dollars. Thus, there is great interest in smaller, cost-effective flow cytometers. In the following report, we detail the design and fabrication of a microfluidic "flow cytometer on a chip," to address this growing need. The device is produced by the fabrication of microchannels and electrodes in a silicon wafer with the incorporation of both hydrodynamic and electrokinetic focusing capabilities.**

I. Introduction

Flow cytometry involves quantifying and discriminating between cells or other particles suspended in an aqueous solution. Often, biological experiments require single-cell measurements. Thus, cells must be analyzed on an individual scale, requiring techniques of microfabrication to produce the stream of individual cells, and requiring fast fluid and detection speeds to measure the properties of large quantities of cells. Traditionally, flow cytometers are bulky machines, intended for laboratory use; however, with the rise of more sophisticated medical techniques/increased need for accessible pathology, smaller-scale flow cytometers present an exciting opportunity. Particularly, utilizing microfabrication/fluidics to produce a chip-scale flow cytometer could bring the power of cellular analysis into a variety of settings, most notably the clinical sphere [1].

To achieve its function, the flow cytometer on a chip must satisfy the two requirements above. It must be able to produce a high speed, very focused stream of fluid with suspended particles (usually cells). To achieve this, a micro-scale device can be constructed to utilize hydrodynamic focusing. This method consists of a fluid inlet stream that is focused by side streams of a sheath fluid. The resulting narrow stream can then be focused with electrodes to create a stream of single cells. Electrokinetic focusing consists of two side electrodes of a given polarity and a middle electrode of the opposite polarity along which the stream is aligned. The layout of the device at a high level can be seen in Fig. 1. The microchannels are produced using standard methods of silicon microfabrication. Wafers are oxidized, coated with photoresist, exposed to UV light with a mask to produce the channel patterns, developed and etched to create the channel in the silicon, re-oxidized to create an insulating layer to isolate the electronic components, coated with aluminum by thermal evaporation, further etched and patterned, and finally sealed in with anodic bonding to a glass plate. This design provides a sophisticated microfluidics approach to flow cytometry [2].

II. Experimental Methods

A. Mask Design

Masks used for photolithography steps were appropriated from previous work. However, the basic principle involved utilizing L-Edit software to produce a computer-aided design (CAD) rendering of the mask geometry. This design was incorporated into photo masks consisting of transparency film on glass, selected for its low cost/ease of production. The choice was justifiable since the feature sizes for the device are large (greater than 10 micrometers) [3]. A dark-field mask was used since a positive photoresist was chosen (for its better resolution and thermal properties) [4].

B. Photolithography I

Refer to Fig.1.2. The first step of fabrication involved photolithography to etch the oxide layer of the silicon wafers, in preparation for microchannel fabrication. Wafers were baked to dehydrate them and thus ensure proper photresist adhesion. Positive photoresist S1813 was then spun on both sides of the wafer (sequentially, with a bake step in between to dry the photoresist). The backside was coated for protection during the etch processes. Wafers were then exposed to UV light with the aforementioned photomask and developed in CD26 developer solution, followed by an additional drying/bake step. Etching was then performed using a buffered oxide etch (BOE) consisting of NH_4F and HF. Due to the caustic nature of the etchant, additional personal protection was used, including thicker chemical-resistant gloves and face shields. Following BOE, the wafer was rinsed to remove excess etchant and the remaining photoresist was removed with acetone. Final surface cleaning was achieved by isopropanol (IPA) soak. Oxide removal was confirmed using profilometer measurements. The oxide was purposely somewhat over-etched in order to confirm complete removal, since the etch rate of the next step is highly selective for silicon over silicon dioxide.

C. Bulk Substrate Etching

Refer to Fig. 1.3. Microchannels were then machined via wet etching of the patterned wafer using potassium hydroxide (KOH). KOH is an anisotropic etchant, which preserves the desired wall structure, creating straight-edged microchannels with minimal undercutting. Wafers were soaked in 30% KOH solution (with added IPA to promote etchant adhesion and

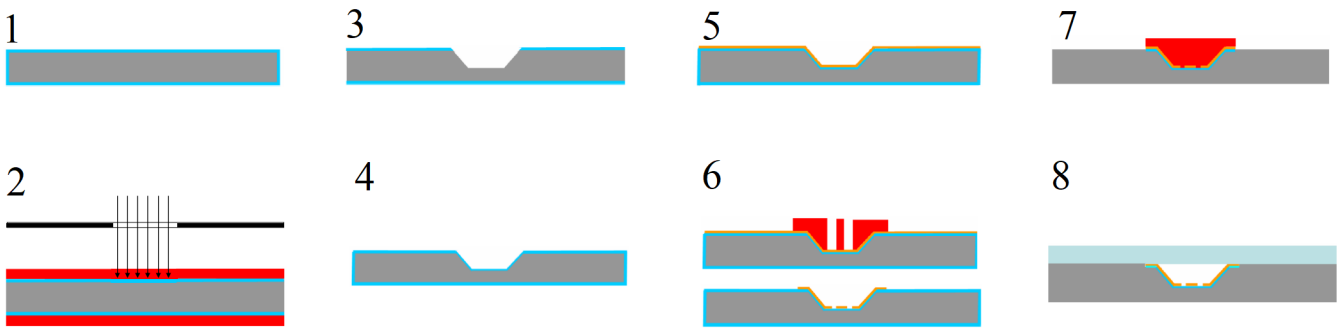

Fig. 1. Process diagram showing each major step. For information on each step, read the corresponding section. Fig. 1.1 (the first process: growing an oxide layer on the bare silicon wafer) was performed before the experiments detailed in this report. The dark gray base shape is the silicon wafer, blue layers are oxide, red is photoresist, orange is aluminum, and light gray is the anodically bonded glass. The images for each step are adapted from [2].

channel smoothness), and etch time was calculated based on previous work by [5]. The time to etch 20 micrometer deep channels was estimated at twenty-four minutes (an etch rate of 50 micrometers per hour). The wafer was soaked for half of this time and removed, followed by measurement with the profilometer to determine the depth of the channel and thus calculate the actual etching rate. Additionally, the oxide thickness was measured using the optical thin-film measurement system in order to correct for oxide etching as well as determine the selectivity of the etch. The actual rate was found to be 48 micrometers per hour, which is within the range of expected variability due to measurement error. The wafer was then soaked for the remaining time. The channels were somewhat rough, which could be improved with increased IPA and/or KOH concentration in the etch.

D. Oxidation

Refer to Fig. 1.4. Next, an oxide layer was regrown over the entire wafer in order to insulate the silicon of the wafer from the electrodes deposited in the next step. First, all of the existing oxide was removed from the wafer via BOE etch. Then, a uniform layer of oxide was grown over the wafer via wet thermal oxidation at 1100 °C. Wet oxidation was chosen for speed. Wafers were slowly pushed into the furnace in a quartz boat to prevent breaking due to rapid temperature change [6].

E. Aluminum Evaporation

Refer to Fig. 1.5. Aluminum was deposited on the top surface of the wafer via thermal evaporation. The wafer was deposited in a vacuum chamber which was pumped down to approximately one microtorr (thereby reducing the boiling point). Additionally, this low pressure substantially increases the mean free path of metal atoms. These atoms then bombard and coat the surface of the wafer, which is positioned in the chamber to receive some amount of ideally uniform flux across its surface. In the case of the present experiment, 0.17 grams of aluminum were deposited in 10 minutes, thus giving a mass loss rate of:

$$R_{ML} = \frac{0.17\ \text{g}}{10\ \text{min}} = 2.833 \times 10^{-7} \frac{\text{kg}}{\text{sec}} \tag{1}$$

Plugging this value in to calculate mass deposition rate gives:

$$R_D = \frac{R_{ML}}{4\pi r^2 \rho} = 8.989 \times 10^{-11} \frac{\text{m}}{\text{sec}} \tag{2}$$

Where r and ρ are the distance between the crucible and wafer and the wafer and the density of the deposition material (aluminum in this case), respectively [7]. The calculated deposited amount, based on this deposition rate, is 539.3 Å. The actual measured amount was found to be 569 Å. Afterwards, the aluminum metal was coated with SPR220-7 photoresist in preparation for aluminum patterning. A very thick layer was applied for substantial protection against the aluminum etchant, which is extremely reactive.

F. Photolithography II

Refer to Fig. 1.6. The photoresist was then patterned via UV exposure with a mask containing the electrode designs and developed in CD26 solution, followed by a hard bake. In this portion of fabrication, the exposure time is much longer than the previous photolithography step because of the much thicker layer of photoresist. Then a PAN etch solution was used to pattern the aluminum, and the photoresist was removed.

G. Photolithography III

Refer to Fig. 1.7. In the next step, oxide was removed from the wafer except for the regions of interest (the electrodes/microchannels). This involved the same process as the previous photolithography steps, including a dehydration bake, spinning on photoresist, UV exposure through a photomask, development in CD26 solution, and etching (this time using BOE, as in Photoloithography I). Finally, the photoresist was removed in acetone and the wafer was cleaned in IPA.

H. Anodic Bonding

Refer to Fig. 1.8. In the final fabrication step, the microfluidic device was sealed using two methods. The primary method involved anodic bonding of borosilicate glass to the top surface of the wafer. This method functions by utilizing heat and an electric potential (thousands of volts) to promote diffusion of ions within the glass. This separation of charge creates an electrostatic attraction of oxygen anions at the

silicon-glass interface, promoting the formation of silicon dioxide at the junction [8]. Thus, the glass cover and the wafer become joined. In practice, this method involved marking the glass slide with the inlet and outlet locations and drilling holes at these points to allow the attachment of tubing. Then, the glass and wafer were clamped together on a 400 °C hot plate while 2000 V were applied [8]. Additionally, a wafer was prepared using polydimethylsiloxane (PDMS). PDMS is a flexible, clear organic polymer used for microfluidics packaging. Following plasma cleaning in an oxygen plasma, the surface contains exposed SiOH groups, which when brought in contact with the plasma-cleaned wafer form bridging Si-O-Si bonds, holding the PDMS onto the wafer [9]. After packaging of both wafer types, testing was performed to determine the effectiveness of the flow cytometers. The completed wafers are visible in Fig. 2.

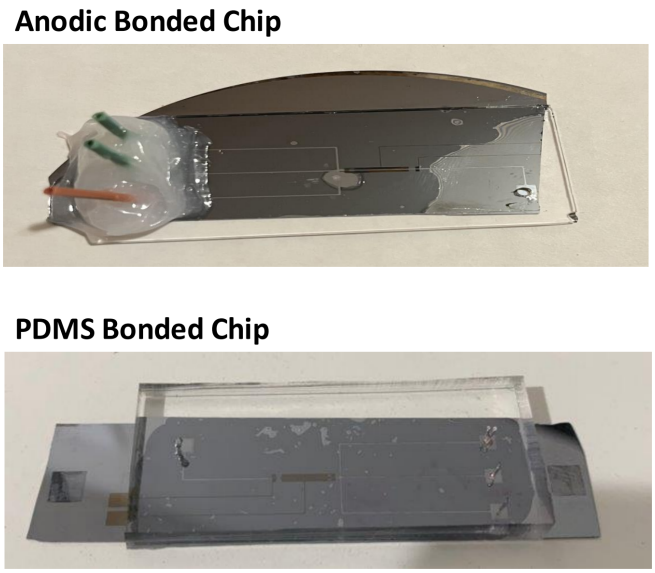

Fig. 2. Final fabricated flow cytometer wafers.

III. Results and Discussion

A. Testing Method

Wafers were tested via manual injection methods and microscope imaging. Three tubes were attached to the inlet (one fluid of interest inlet, for which we used green dye, and two sheath fluid inlets, for which we used deionized water), and syringes filled with fluid were attached to the other end of each tube. Three individuals then balanced fluid flow rates with manual compression of the syringes to produce a laminar stream of dye, which was imaged via optical microscope with a video camera. This process was performed on both the glass-packaged chip and the PDMS-packaged one. Despite the capability of performing electrokinetic focusing, this functionality was not utilized for testing the wafers.

B. Anodic Bonding Results

The wafer packaged with anodically bonded glass functioned well, achieving a thin, focused stream of dye with precise control of the sheath fluid. There were some issues in the bonding process, as the bonding took substantially longer than anticipated, and there was a small amount of leakage/air pockets within the silicon-glass interface (as can be seen in the first panel of Fig. 2). Additionally, achieving the balance between sheath fluid flow rates and the dye stream flow rate was challenging, given the individual control of each of the three inlets. However, successfully focusing was achieved by careful visual inspection of the quality, thickness, and direction of flow of the dye stream, which allowed for adjustment of the three flow rates in real time. For future improvements, an automated injection device may produce significantly more reliable results.

C. PDMS Bonding Results

The wafer packaged with plasma-bonded PDMS failed to function. The seal between the wafer surface and the silicon was extremely poor, causing substantial leakage to occur, with liquid pooling underneath the PDMS and eventually leaking out of the sealed interface around the inlets. Likely, there was some error in the bonding process (perhaps the sides were insufficiently cleaned/prepared for bonding in the plasma treatment). There was human error in the first attempt at PDMS bonding (the wrong, untreated side of PDMS was actually placed on the wafer surface); however, the process was repeated with an extra wafer without any identifiable human error, yet there was still a poor seal. A full diagnosis/audit of the packaging process would be necessary to determine the source of this error in PDMS bonding.

D. Conclusion

Over the course of eight weeks, a flow-cytometer on a chip microfluidics device was fabricated and tested. A successful device was produced, along with some failed attempts. Nevertheless, the methods disclosed in this report provide a framework for producing low-cost, small-footprint flow cytometer devices that can bring the power of microscale analysis into the hands of researchers, clinicians, and enthusiasts everywhere, without the need for a laboratory and associated lab funding.

References

[1] Gawad, S., Valero, A., Braschler, T., Holmes, D., Renaud, P. (2012). "On-Chip Flow Cytometry." In: Bhushan, B. (eds) "Encyclopedia of Nanotechnology." *Springer*, Dordrecht.

[2] Andreou, A. and Wang, J. (2022). "Introduction to Fabrication and Project" [PowerPoint slides]. Johns Hopkins University Microfabrication Lab Canvas: https://jhu.instructure.com/

[3] Andreou, A. and Wang, J. (2022). "Photolithography I" [PowerPoint slides]. Johns Hopkins University Microfabrication Lab Canvas: https://jhu.instructure.com/

[4] Andreou, A. and Wang, J. (2022). "Photolithography II" [PowerPoint slides]. Johns Hopkins University Microfabrication Lab Canvas: https://jhu.instructure.com/

[5] Seidel, H. (1987). "The mechanism of anisotropic silicon etching and its relevance for micromachinings", in *Research and Development. Technical-Scientific Publications (1956-1987): Retrospective View and Prospects. Jubilee Edition on the Occasion of the 75th Anniversary of Dipl.-Engr. Dr.-Engr. E.H. Ludwig Boelkow*, pp. 127–130.

[6] Andreou, A. and Wang, J. (2022). "Thermal Oxidation" [PowerPoint slides]. Johns Hopkins University Microfabrication Lab Canvas: https://jhu.instructure.com/
[7] Andreou, A. and Wang, J. (2022). "Thin Film Deposition" [PowerPoint slides]. Johns Hopkins University Microfabrication Lab Canvas: https://jhu.instructure.com/
[8] Andreou, A. and Wang, J. (2022). "Packaging" [PowerPoint slides]. Johns Hopkins University Microfabrication Lab Canvas: https://jhu.instructure.com/
[9] Borók, A., Laboda, K., and Bonyár, A. (2021). "PDMS Bonding Technologies for Microfluidic Applications: A Review." *Biosensors*, 11(8), 292. https://doi.org/10.3390/bios11080292